Available online at www.ijournalse.org

Emerging Science Journal

(ISSN: 2610-9182)

Vol. 6, No. 4, August, 2022

Vector Control of Asynchronous Motor of Drive Train Using Speed Controller H_∞

Abdelhak Boudallaa [1*], Mohammed Chennani [2], Driss Belkhayat [2], Karim Rhofir [2]

[1] *National School of Applied Sciences Khouribga, University of Beni Mellal, Morocco.*

[2] *Faculty of Sciences and Technologies, University of Marrakesh, Morocco.*

Abstract

This study proposes the speed control of an asynchronous motor (AM) using the H_∞ Antiwindup design. First, the conventional vector control based on proportional-integral (PI) controllers is developed for a constant speed set point. Then, a driving cycle is based on measurements on the Safi/Rabat motorway in Morocco using a microcontroller equipped with a GPS device. The collected practical speed is used as a speed reference for conventional vector control. The H_∞/Antiwindup controller of the direct rotor flow-oriented control is used to improve the performance of conventional vector control and optimize the energy consumption of the drive train. The effectiveness of the proposed control scheme is verified by numerical simulation. The results of the numerical validation of the proposed scheme showed good performance compared to conventional vector control. The speed control systems are analyzed for different operating conditions. These control strategies are simulated in the MATLAB/SIMULINK environment. The simulation results of the improved vector control of the Asynchronous Machine (AM) are used to validate this optimization approach in the dynamic regime, followed by a comparative analysis to evaluate the performance and effectiveness of the proposed approach. A practical model based on a TMS320F28379D embedded board and its reduced voltage inverter (24V) is used to implement the proposed method and verify the simulation results.

Keywords:

Electric Vehicle; PI/H_∞;
Antiwindup Controller;
Induction Motor;
Vector Control;
Matlab/Simulink;
dSpace Board TMS320F28379D.

Article History:

Received:	20	February	2022
Revised:	04	April	2022
Accepted:	17	May	2022
Available online:	31	May	2022

1- Introduction

Electric vehicles (EVs) have been considered a good vehicle choice for reducing greenhouse gas emissions. However, the relatively short range of most commercially available electric vehicles limits their efficiency. Before energy density increases significantly, improving the overall powertrain efficiency of electric vehicles is a cost-effective and practical way to increase their use. At the same time, electric vehicle powertrain efficiency reduces electrical energy consumption. Multi-speed transmissions have been widely used in traditional internal combustion engine vehicles for two reasons:

- Firstly, multi-speed transmissions provide better dynamic performance for vehicles (i.e., higher top speed, faster acceleration, and smoother starting).
- Secondly, they allow vehicles to operate at high efficiency through gear shifting, which reduces fuel consumption. However, there are few electric vehicles with multi-speed transmissions [1].

In the context of the electric vehicle, research has been and is being carried out on the various parts of the powertrain. Since the significant appearance of the electric vehicle, the DC machine has been the most widely used. One of the main

* **CONTACT**: boudallaa.abdelhak@gmail.com

DOI: http://dx.doi.org/10.28991/ESJ-2022-06-04-012

challenges is the acquisition of important data, the position of the vehicle on the road, and its speed in relation to a specific mission or use. The idea is, therefore, to take into account the actual mission of the vehicle in order to optimize the powertrain rather than set specific performance requirements (maximum speed, acceleration, range).

Ye et al. (2016) developed a hybrid approach for estimating the energy consumption of electric vehicles [2]. It combines the knowledge-based model of Wu et al. (2015) [3] and the data-based model of Yao et al. (2014) [4]. Knowledge-based variable selection based on an analytical model is often a source of estimation in terms of real-time performance due to its complexity. On the contrary, data-based variable selection does not necessarily consider their physical meaning, which leads to unsatisfactory predictability and scalability because it is customized by specific training datasets.

Optimal energy management is one of the many critical aspects of advancing fuel Cell/Super-capacitor hybrid electric vehicle technologies. Characterized by the slow dynamic response, a fuel cell system is unable to meet the transient demand for motive power. Hybridization with another auxiliary source, such as a battery and/or Super-capacitor module, is crucial to the dynamic performance of the system. However, the development of a power management system and control strategy is necessary to ensure optimal performance according to the system characteristics and constraints.

Lü et al. (2018) presented a comparative study of four real-time energy management strategies, applied to hybrid electric petroleum vehicles, and fuel cell electric vehicles. Optimization methods such as Pontriagin's minimum principle and dynamic programming are applied and implemented to provide results. The problems of numerical implementation and parameterization of the strategies are also discussed [5]. Satisfying the traction power is the main role of the EMS, however, solving only the power distribution problem is not enough. Fuel economy, system dynamics, and durability are also other key criteria for optimal performance. However, in order to combine multiple objectives, powerful strategies must be developed. An appropriate EMS is expected to achieve optimal power distribution of the hybrid source, maintain system durability, reduce hydrogen consumption and ensure user safety.

Several research papers have considered a multi-objective scheme. However, some papers focus only on one or two criteria without considering the other aspects [6, 7]. The proposed management approaches can be mainly classified into classical rule based techniques and advanced optimization based techniques. The classical techniques are simple to implement and do not require optimal performance. On the other hand, optimization-based methods are more complex and therefore require more effort and computation time. But they are able to achieve optimal performance for a given cost and associated constraints.

Online energy management based on a data fusion approach has been studied before [7], where fuzzy logic controllers are optimized according to the trapezoidal fit. The proposed method considers different driving cycle models for the fuel-cell/Super-capacitor hybrid electric vehicle and assigns a specific optimization objective for each driving cycle. The randomness of the driving cycle of electric vehicle requires a more accurate but real-time control strategy. Kumar & Moulik (2021) [8] present a comparison of the most commonly used electric motors and their control techniques for electric vehicles.

Wei et al. (2022) developed a dynamic energy management strategy for EVs to optimize battery energy consumption and simultaneously reduce tire slip loss [9]. Non-linear model predictive control is used to identify tire dynamics and vehicle load. All these elements motivated the writing of this paper for an in-depth study of rotor flow-oriented vector control whose objective is to improve the dynamic performance of the system during speed variation on a real trajectory [10].

To validate our controller H_∞ approach, for an induction machine speed controller based on the flux orientation strategy. This strategy is simulated in Matlab/Simulink and then implemented using a TMS320F379D embedded board. In order to demonstrate the superiority of the proposed H_∞ control, its performance was compared with that of a conventional PI-based direct vector control under different operating conditions [11]. The vector control is based on velocity measurement. However, physical sensors have shortcomings that can degrade system control.

Indeed, the cost of the sensors can considerably increase the total cost of a control system, and their associated wiring reduces the reliability of the control system, for which a classical MRAS speed estimator is used and improvements by other types of more efficient speed estimators are planned. The objective of this paper is to compare the performance of PI and H_∞ controllers applied to an asynchronous motor in order to propose an efficient solution to minimize the energy consumption of the vehicle when moving along a well-defined trajectory.

This study is organized into five sections. Section 2 presents the description of the powertrain and its dynamic modeling, and then a practical microcontroller-based system is developed to collect geographical data from the vehicle on the road. Section 3, describes the design of the conventional vector control based on proportional-integral (PI) controllers, section 4, describes the modeling of the asynchronous motor and the conventional and robust control techniques H_∞ applied to the vector control, section 5, presents a comparative study of the dynamic performance of the two methods the practical test bench used to implement the control techniques.

In perspective, advanced control techniques such as Pontriagin's minimum principle are considered for application to the asynchronous motors of the drive train are under development and implementation using the DSP TMS320F28379D board and its reduced voltage (24V) inverter.

2- Traction Chain

2-1- Description

The wheels are connected to the induction machine for mechanical transfer (Figure 1). The motor is powered by a three-phase inverter, which converts direct current into alternating current. The direct current comes from a DC-DC converter powered by rechargeable batteries.

Several types of powertrains have been developed to power vehicles [6]:

- Internal combustion vehicle;
- Hybrid vehicle;
- The plug-in hybrid vehicle;
- Electric vehicle (EV).

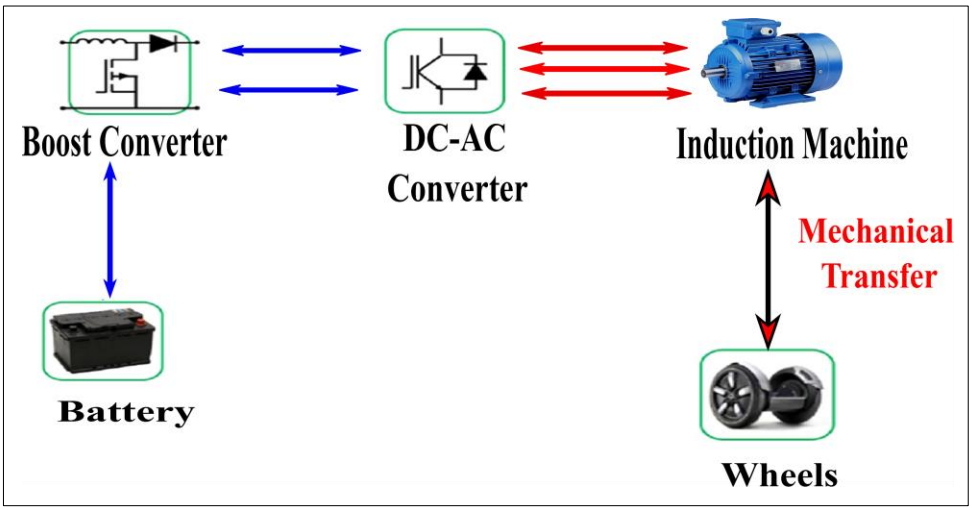

Figure 1. Energy conversion chain

2-2- Experimental Model Based on the GPS On-Board System

The driving cycle is based on measurements made on the Safi/Rabat motorway in Morocco, using a microcontroller model equipped with a GPS module. The actual measurements allow the speed profile to be plotted according to time (Figure 1), and the validity of the results to be verified by plotting the route on a MAPS map (Figure 2) [10].

The data collected in the table (Table 1) represent part of the data collected while the vehicle was running for four hours without stopping on the A1 motorway in Morocco (from 14h, 18min to 18h, 16min).

Table 1. Recorded data

Latitude	Longitude	Altitude (m)	Speed (Km/h)	Time / Date
32.29699	-9.214521	113.9	0	14:18:53 / 13.05.2020
32.29787	-9.213886	113.9	28.5	14:19:08 / 13.05.2020
32.2984	-9.213513	113.7	28.5	14:19:24 / 13.05.2020
…….	…….	…….	…….	…….
32.8874	-9.813513	102.5	74.5	16:19:24 / 13.05.2020
…….	…….	…….	…….	…….
33.95274	-6.914687	70.8	95.4	18:15:30 / 13.05.2020
33.9549	-6.914562	72.5	70.8	18:15:48 / 13.05.2020
33.95707	-6.910218	73.6	91.3	18:16:05 / 13.05.2020

To validate the data collected by our GPS system (table 1), the Safi/Rabat trajectory travelled by the vehicle is shown in Figure 2.

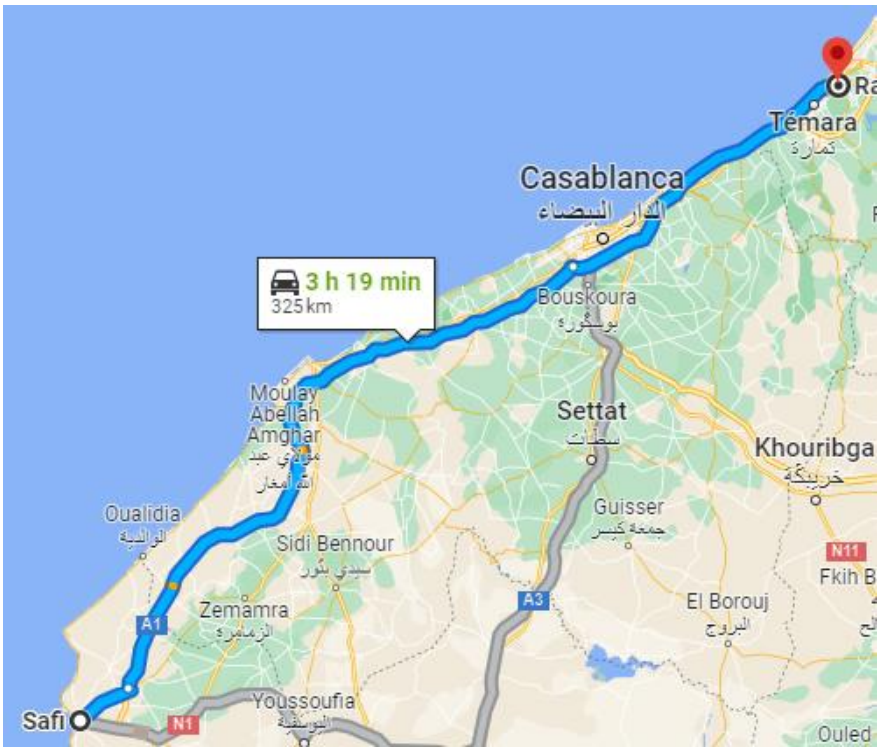

Figure 2. The itinerary between Safi and Rabat

2-3- Force Applied to the Vehicle

The vehicle is considered as a moving solid point body subject to three forces along the longitudinal axis (Ox), Figure3.

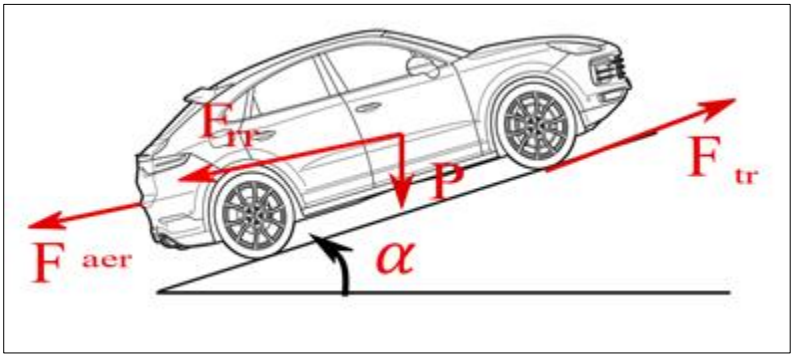

Figure 3. Forces applied to a vehicle

- The traction force results from the action of the driving wheels on the road surface.
- The aerodynamic drag force.
- The resistance to elevation:

The fundamental principle of vehicle dynamics:

$$M_{veh}a_{veh} = F_{tr}(t) - F_{aer}(t) - F_{rr}(t) \quad (1)$$

2-4- The Wheels

The wheels are mechanical force converters. The torque delivered by the rotating powertrain is transformed into forces applied to the vehicle body [12]. The model considered is therefore a simplified model, which only takes into account the resultant of the forces generated by the four tyres. A single virtual wheel is therefore sufficient to represent the average behaviour of the four wheels.

This virtual wheel generates a driving force F_{mot} (t) from the wheel torque delivered by the drive train.

$$F_{mot}(t) = \frac{C_{wheel}(t)}{R_{wheel}} \quad (2)$$

The interface between the tyre and the road surface is the seat of frictional forces Froll (t) which oppose the progress of the vehicle:

$$F_{roll}(t) = M_{veh}.g.C_r(V_{veh}(t)).\cos(\alpha(t)) \quad (3)$$

The coefficient of friction C_r depends on the vehicle speed V_{veh}. For given operating conditions (temperature, humidity) and within the framework of an energy model, we obtain a quadratic function:

$$C_r(V_{veh}) = C_r^0 + K_{cr}.V_{veh}^2(t) \quad (4)$$

where; C_r^0 and K_{cr} are coefficients that can be determined experimentally.

Finally, the tensile force applied to the drive train is written as follows:

$$F_{tr}(t) = F_{mot}(t) - F_{roul}(t) \quad (5)$$

The speed of rotation is given by:

$$\omega_{weel}(t) = \frac{V_{veh}(t)}{R_{wheel}} \quad (6)$$

2-5- Gearbox and Transmission

The gearbox adapts the speed and torque between the electric machine shaft (ω_{mot}, C_{mot}) and the drive wheels (ω_{wheel}, C_{wheel}).

The transmission is mainly composed of the differential block, which is responsible for distributing the output torque of the gearbox evenly to the driving wheels. An overall reduction ratio is considered between the electric machine shaft and the wheel. The efficiency of the gearbox/transmission assembly is assumed to be constant. According to the assumptions made, the relationships between torques and speeds are given by:

$$\omega_{mot}(t) = \omega_{wheel}(t) r_{red} \quad (7)$$

3- Mathematical Model and Control Technique for IM Drives

The asynchronous motor fed by a voltage inverter is considered the main actuator in the electric drive train, subsequently; simulation work was carried out to optimize the energy consumption of all the train components using a speed estimator (MRAS).

Et-Taaj et al. (2021) developed a robust sensorless control of the induction motor (IM) using the extended Kalman filter (EKF) [13], the quality of speed estimation depends strongly on the rotor and stator resistance. A change in the rotor or stator resistance causes a significant speed estimation error, especially at low speeds. The variation of these resistances affects not only the estimated speed but also the indirect vector control.

3-1- Mathematical Model of the Induction Motor

The dynamic mathematical model of the induction motor consists of the differential equations describing the electromagnetic relations of the stator and rotor and the equation of motion [11, 14].

The Equations 9 to 13 describe the dynamic model of the induction motor:

$$\frac{dI_s^d}{dt} = -\left(\frac{1}{\sigma T_s} + \frac{1-\sigma}{\sigma T_r}\right) I_s^d + \omega_s I_s^q + \left(\frac{1-\sigma}{\sigma M T_r}\right) \Phi_r^d + \left(\frac{1-\sigma}{\sigma M}\right) \omega \Phi_r^q + \frac{1}{\sigma L_s} V_s^d \quad (9)$$

$$\frac{dI_s^q}{dt} = -\omega_s I_s^d - \left(\frac{1}{\sigma T_s} + \frac{1-\sigma}{\sigma T_r}\right) I_s^q - \left(\frac{1-\sigma}{\sigma M}\right) \omega \Phi_r^d + \left(\frac{1-\sigma}{\sigma M T_r}\right) \Phi_r^q + \frac{1}{\sigma L_s} V_s^q \quad (10)$$

$$\frac{d\Phi_r^d}{dt} = \frac{M}{T_r} I_s^d - \frac{1}{T_r} \Phi_r^d + (\omega_s - \omega) \Phi_r^q \quad (11)$$

$$\frac{d\Phi_r^q}{dt} = \frac{M}{T_r} I_s^q - (\omega_s - \omega) \Phi_r^d - \frac{1}{T_r} \Phi_r^q \quad (12)$$

$$C_e - C_r = J_m \frac{d\Omega}{dt} + f_m \Omega \ \ avec \ C_e = \frac{3M}{2Lr} P(\Phi_{rd} I_{sq} - \Phi_{rq} I_{sd}) \quad (13)$$

3-2- Rotor Speed Estimation

The MRAS method is based on the comparison of the outputs of two estimators. The first, called the reference model, does not depend on the quantity to be estimated and the second, the adjustable model, depends explicitly on the quantity to be estimated. The error between the outputs of the two estimators drives an adaptation mechanism that generates the estimated speed ω_r.

3-2-1- MRAS Reference Model

The components of the flux Φ_s from the measurement of the stator currents. The measurement of the stator currents i_s and stator voltages as a function of the stator flux can be derived from the following relationship [9, 10].

$$\begin{aligned} \Phi_{\alpha s} &= \int_0^t (v_{\alpha s} - R_s i_{\alpha s})dt \\ \Phi_{\beta s} &= \int_0^t \left(v_{\beta s} - R_s i_{\alpha\beta}\right)dt \end{aligned} \tag{14}$$

3-2-2- MRAS Adjustable Model

Based on the rotor equations, it is shown that [10]:

$$\begin{aligned} 0 &= -L_s(R_r + p\sigma L_r)i_{\alpha s} - \sigma L_r L_s \omega_r i_{\beta s} + (R_r + pL_r)\phi_{\alpha s} + \omega_r L_r \phi_{\beta s} \\ 0 &= \sigma L_r L_s \omega_r i_{\alpha s} - L_s(R_r + p\sigma L_r)i_{\beta s} - \omega_r L_r \phi_{\alpha s} + (R_r + pL_r)\phi_{\beta s} \end{aligned} \tag{15}$$

The system (15) can be expressed as follows:

$$\begin{aligned} \hat{\phi}_{\alpha s} &= \frac{\tau_r}{1+\tau_r p} + \left(\sigma L_s \omega_r i_{\beta s} + \frac{L_s}{\tau_r}(1 + \sigma\tau_r p)i_{\alpha s} - \omega_r \hat{\phi}_{\beta s}\right) \\ \hat{\phi}_{\beta s} &= \frac{\tau_r}{1+\tau_r p} + \left(-\sigma L_s \omega_r i_{\alpha s} + \frac{L_s}{\tau_r}(1 + \sigma\tau_r p)i_{\beta s} + \omega_r \hat{\phi}_{\alpha s}\right) \end{aligned} \tag{16}$$

$$\begin{cases} \varepsilon_\alpha = \phi_{\alpha s} - \widehat{\phi}_{\alpha s} \\ \varepsilon_\beta = \phi_{\beta s} - \widehat{\phi}_{\beta s} \end{cases} \tag{17}$$

The observed error between the states of the two models given by Equation 18 is used to generate ω_r using a proportional-integral controller as an adaptation mechanism (Figure 4).

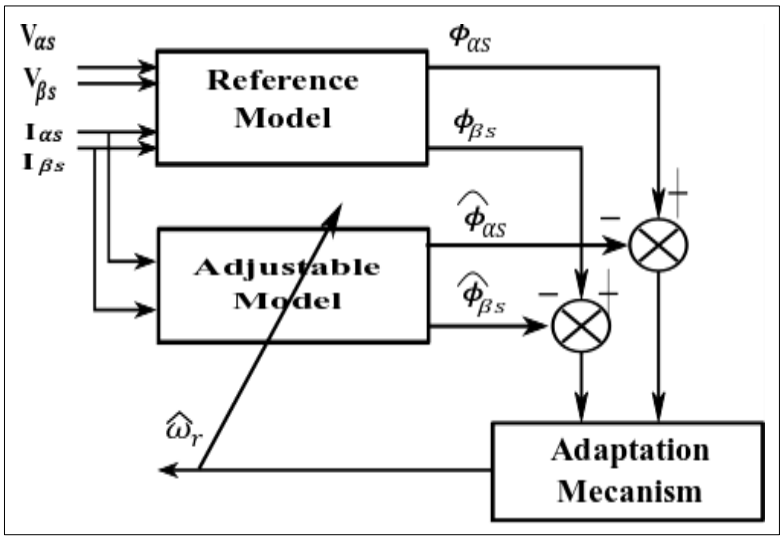

Figure 4. Classical MRAS model

To improve the conventional MRAS, sensorless vector control of the induction motor based on an improved adaptive Luenberger observer is developed. Boulghasoul et al. (2020) propose an observer to estimate both the speed and the parameters of the motor from the measured stator currents, the stator voltages, and the estimated rotor fluxes [15].

3-3- Sensorless Vector Control of an Asynchronous Machine

Equations 9 to 18 can be used to implement sensorless rotor flux vector control of induction machines (Figure 5).

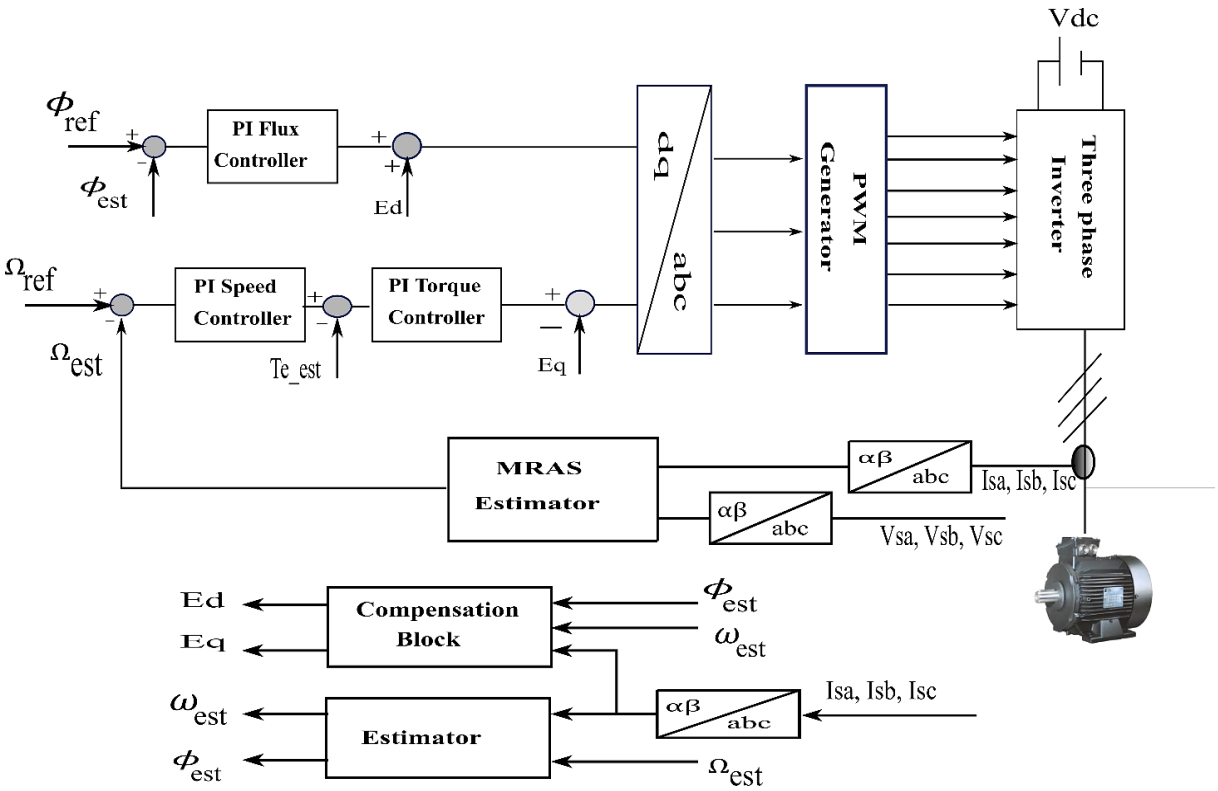

Figure 5. Synoptic diagram of the speed sensorless vector control strategy

3-4- Design of the Proposed Controller Based on the Robust Theory H_∞

The proposed controller is designed to achieve the following objectives:

- Minimal effect of high-frequency measurement noise.
- The maximum limitation of closed-loop signals to avoid saturation.
- Minimal effect of rejecting load disturbances, reducing the peak speed trough.
- Asymptotic and good tracking of sudden changes in control signals, in addition to a fast and excellent damping response.
- Excellent damping response.
- Survival to variations in system parameters.
- H-theory offers a reliable procedure for the synthesis of control signals.

H_∞ Theory provides a reliable procedure for synthesizing a controller that optimally verifies the singular value loop shaping specification [16, 17]. The standard configuration of the control problem H_∞ is to find a static or dynamic feedback controller such that the norm H_∞ (a standard quantitative measure of the size of the system uncertainty) of the closed-loop transfer function is less than a given positive number under the singular value constraint.

The synthesis H_∞ is carried out in two stages:

Formulation: The first step is to select the optimal weighting functions. Appropriate selections of the weighting functions allow the robustness of the system to be improved under different operating conditions and by varying the model parameters. In addition, this allows disturbances and noise to be rejected in addition to parameter uncertainties.

Solution: The weighting transfer function has been updated to the optimal configuration.

In this paper, the MATLAB optimization toolkit in Simulink is used to determine the best weighting functions.

Figure 6 shows the block diagram of the H_∞ design problem, where G(s) is the transfer function of the nominal system of Gp(s) plus weighting functions that represent the characteristics and objectives of the design, u is the control signal and w is the exogenous input vector, which typically includes control signals, disturbances and environmental disturbances and measurement disturbance, and y represents the inputs to the controller, the measurement output and z is the error the output has to minimize.

The objective of this problem is to design a controller K(s) for the augmented system G(s) to have desirable characteristics for the transfer function based on the information from y, to generate the control signal u.

In conclusion, the design problem of H_∞ can be summarised as follows: detect a control law for u (s) = K(s) y(s) to neutralise the effect of w and z and thus minimise the closed loop error.

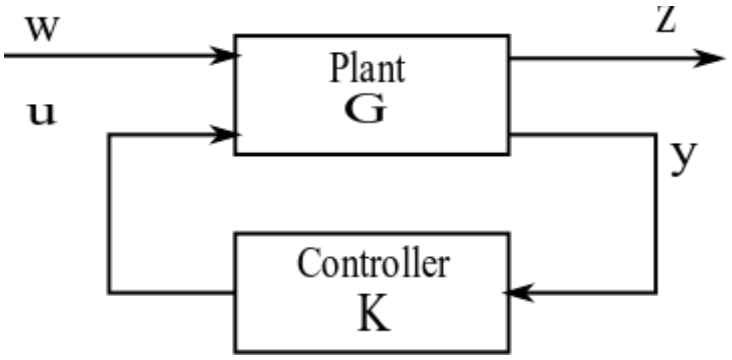

Figure 6. General configuration of the design problem H_∞

In the proposed control system which includes the controller H_∞, the nominal system $G_P(s)$ is augmented by weighting transfer functions $W_1(s)$, $W_2(s)$, and $W_3(s)$, which limits the error signals, control signals and output signals respectively. An incorrect weighting function may lead to poor dynamic performance and instability characteristics of the system.

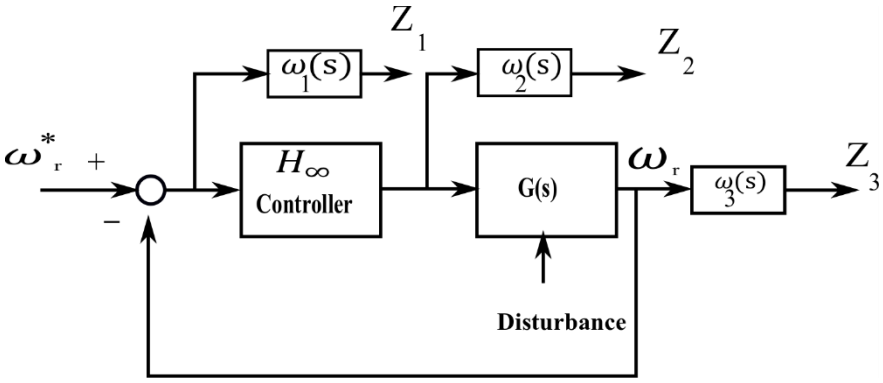

Figure 7. Plant with weighting functions for H_∞ design

Consider the augmented system shown in Figure 7. The set of weighting transfer functions to represent the robustness and performance objectives. A good choice for $W_1(s)$ is useful to obtain a good tracking of the input reference and a good disturbance rejection. The weighted error transfer function matrix Z_1, which is needed for control, can be calculated as follows:

$$Z_1 = W_1(s)[\omega_{ref} - \omega_r] \quad (18)$$

An appropriate selection of the second weighting $W_2(s)$ will exclude actuator saturation and ensure robustness to additional system disturbances.

$$Z_2 = W_2(s).u(s) \quad (19)$$

where; u(s) is the transfer function matrix of the H_∞ controller control signal output.

In addition, an appropriate selection of the third weighting $W_3(s)$ will limit the bandwidth of the closed loop and provide robustness to multiplicative disturbances of the system output and sensor noise at high frequencies. The weighted output variable can be provided as follows:

$$Z_3 = \omega_r W_3(s) \quad (20)$$

In summary, the transfer functions that determine the behaviour of closed-loop voltage and power systems are as follows:

- **Sensitivity function: S**

$$S = [I - G(s).K(s)]^{-1} \quad (21)$$

where G(s) and K(s) are the transfer functions of the nominal system and the H_∞ controller, respectively, while I is the identity matrix. Therefore, when S is minimized at low frequencies, it provides perfect tracking and disturbance rejection.

- **Controller function**

$$C = K(s)[I - G(s).K(s)]^{-1} \quad (22)$$

The minimization of C avoids saturation of the actuator and provides robustness to additional disturbances of the system.

- **Additional function**

$$T = I - S \quad (23)$$

Minimizing T at high frequencies will ensure robustness to multiplicative disturbances of the system output and will allow for noise attenuation.

3-5- Simulation Results and Discussion

The following simulations are carried out to validate the direct rotor vector control of the PWM inverter-driven induction machine, using the vehicle speed reference made in section 2.4 and the flux reference Q_{rd} =0.85Wb.

3-5-1- The Traction Chain on the Marrakech-Safi Route

Using the measurements in Table 1, and the Equations in 1 to 8, the speed profile of the vehicle between Safi and Rabat can be plotted, as well as the power developed by the wheels along the route.

Figures 8-a and 8-b shows the responses of the speed and the power transmitted to the wheels on the Safi/Rabat motorway, and Figure 9 shows the Simulink file of the program used to simulate the electric vehicle.

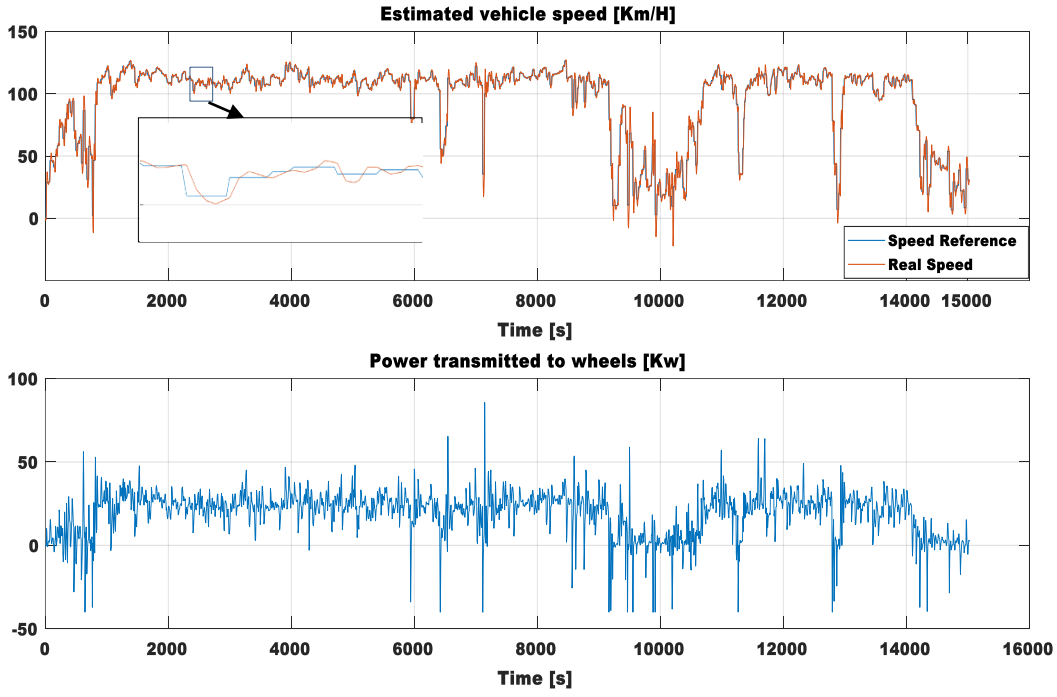

Figure 8. The speed and the power transmitted to the wheels on the Safi/Rabat motorway

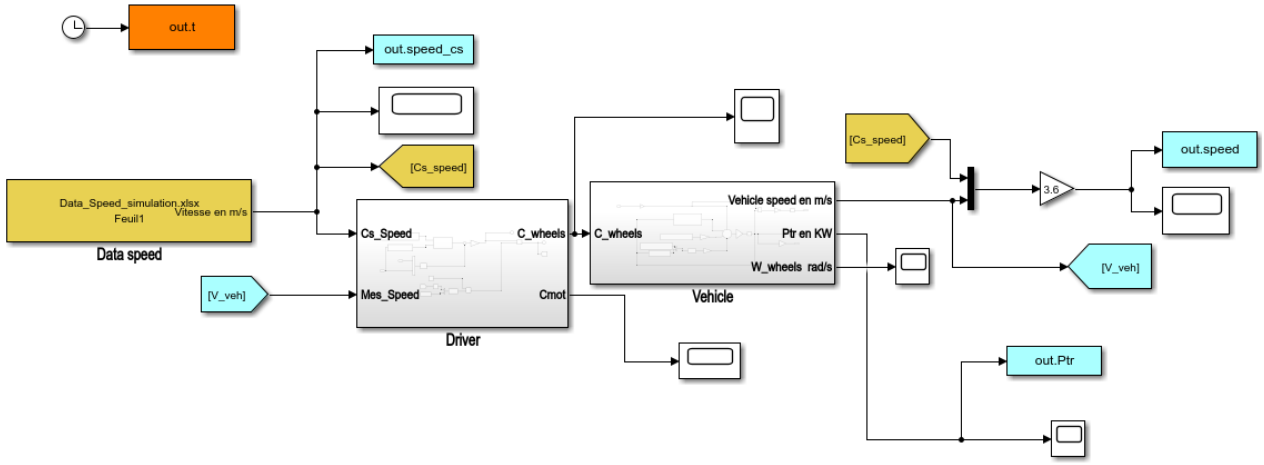

Figure 9. Electric vehicle Simulink program

For a constant speed on the motorway between the instants 1500 and 8000 seconds, the power transmitted to the wheels presents weak undulations, after this instant, the vehicle leaves the motorway and enters the interior of Casablanca, the power decreases and presents quite remarkable undulations because of the acceleration and deceleration of the speed inside the city.

3-5-2- Vector Control with PI Controllers

The simulation of the vector control shown in Figure 10, in the Matlab/Simulink environment, this control is applied to the asynchronous motor, which is used as the actuator of the electric vehicle.

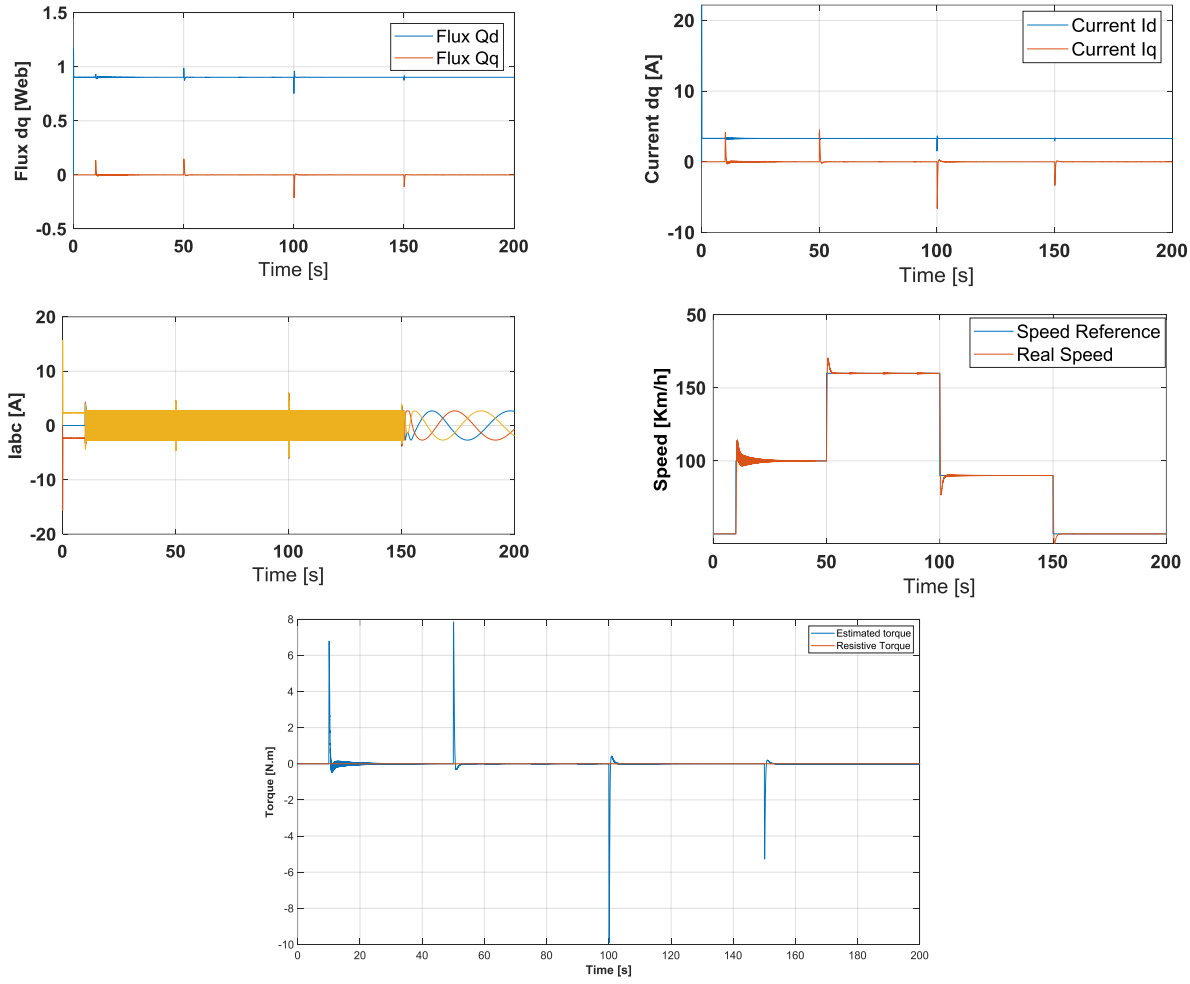

Figure 10. Response of the quantities (Flux, Currents, speed, and electromagnetic torque) of the MAS in the case of classical vector control

3-5-3- Application of H_∞/Anti Windup Control to Rotor Flux Vector Control

The complete block diagram of the field-oriented induction motor drive with the proposed MRAS speed estimator is shown in Figure 11, with the H_∞/Antiwindup controller used to control the speed

The proposed system has been simulated using MATLAB/Simulink under different operating conditions. The following set of weighting functions is obtained using MATLAB/Simulink optimization toolkit to achieve the proposed robustness and performance objectives.

$$\begin{aligned} W_1 &= \mathrm{tf}(1e^2 * [0.1\ 1e^2], 1e^2 * [1e^2\ 0.1]) \\ W_2 &= 0.05 \\ W_3 &= \mathrm{tf}(0.01 * [0.01\ 0.01], 100 * [0.01\ 0.01]) \end{aligned} \tag{24}$$

The corrector obtained by the method is the result of the algorithm described above takes the following form:

$$K_{speed}(s) = \frac{1289s^3+3{,}426.10^5\,s^2+3{,}413.10^5\,s+0.09439}{s^4+1916s^3+4{,}388s^2+4{,}373.10^5\,s+436.9} \tag{25}$$

For which the looped system ensures a standard H_∞ equal to: $\gamma = 0.0397$.

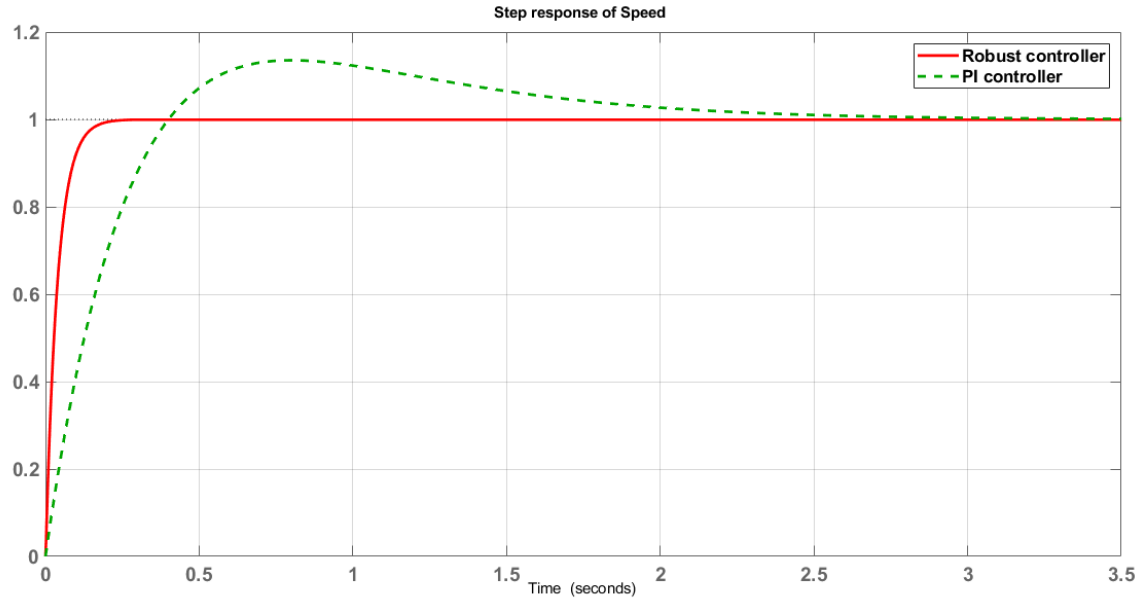

Figure 91. Speed response for two types of controllers

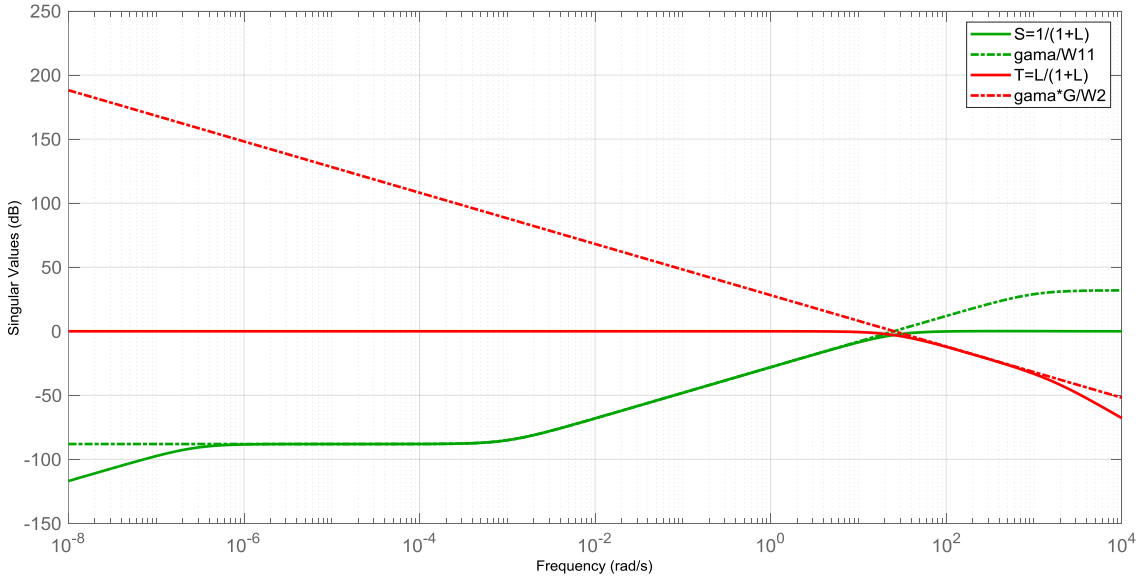

Figure 102. Singular value of functions S, C

The H_∞ control method is one of the most widely used techniques for the design of robust controllers. One of the great advantages of this technique is that it allows the designer to approach the most general form of the control system in which explicit consideration of uncertainties, disturbances, actuator/sensor constraints, actuator and performance measures.

This technique is different from other methods such as LQR and LQG. However, a major disadvantage is the ability required to design the form of the weighting functions and the fact that the process can scale up, the success of the method depends on the correct choice of the weighting transfer function.

3-5-4- Simulation Results of Robust Controlled Driving System with Asynchronous Machine

The simulation results of a drive system controlled by an H_∞ controller show the advantage of using a robust control in applications with a permanent variation of system parameters or external disturbances. A structure of the variable speed with a rotor-flux-oriented control, of the drive train, fed by a PWM voltage source inverter is shown in Figure 13. The rotor position information is obtained from a speed estimator. The control system was simulated in the Matlab / Simulink environment. The speed controller was designed and simulated using several optimization criteria, to be compared with a PI controller.

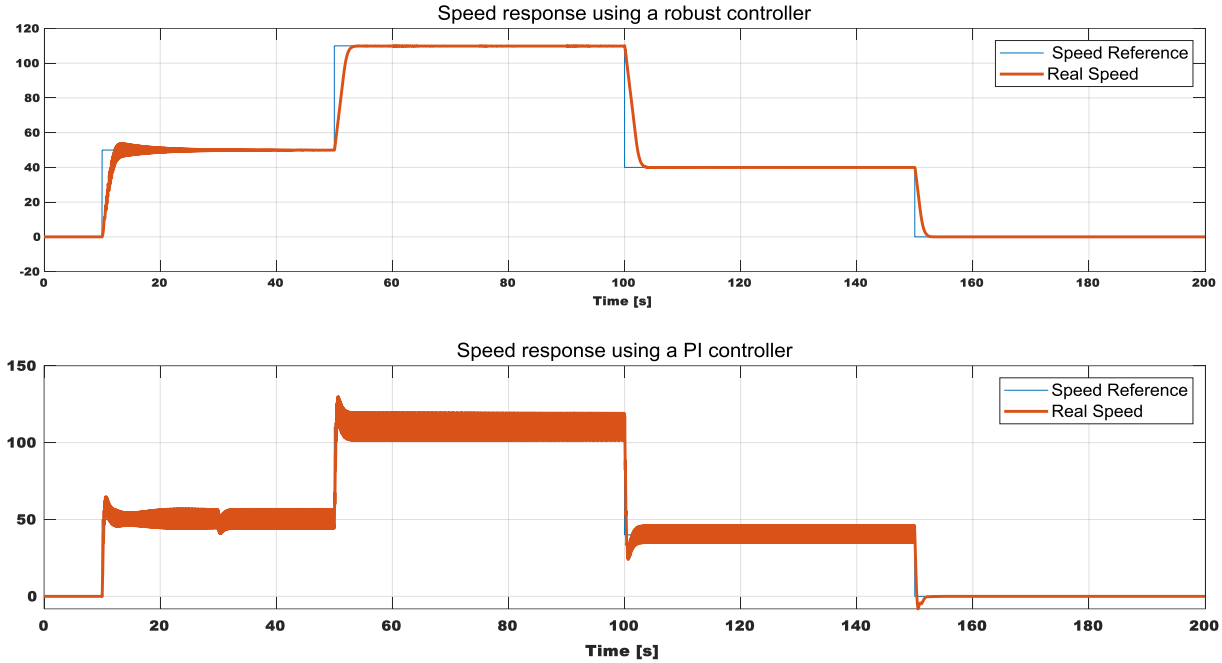

a) Speed Responses

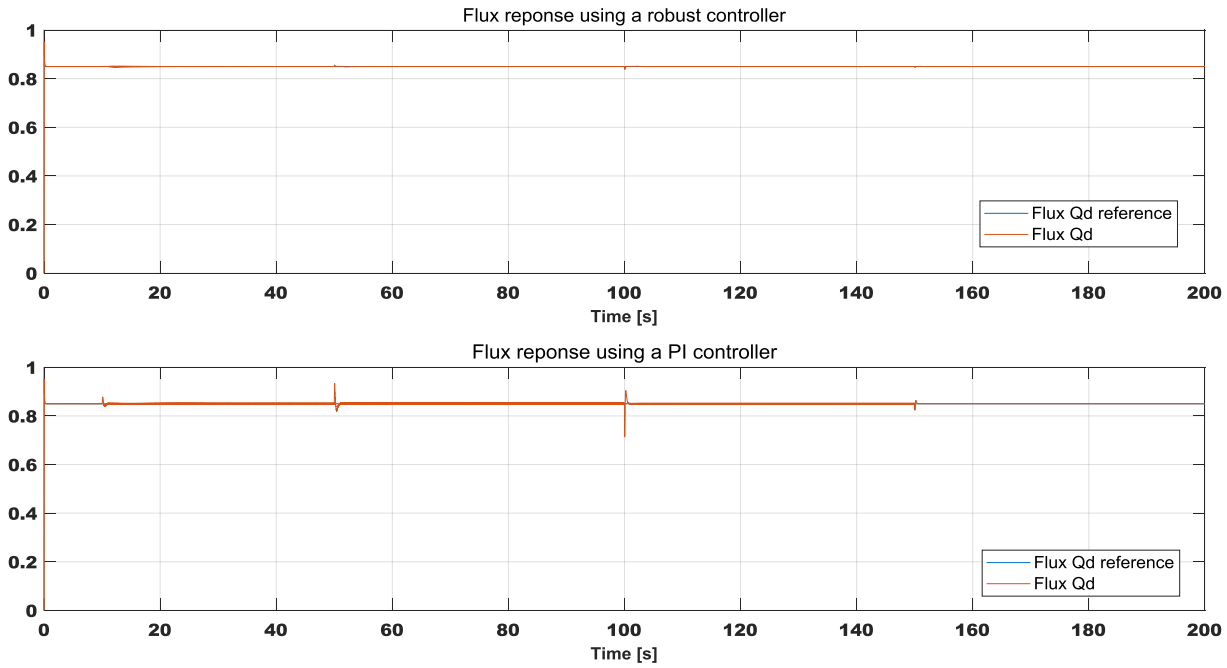

b) Flux responses en [web]

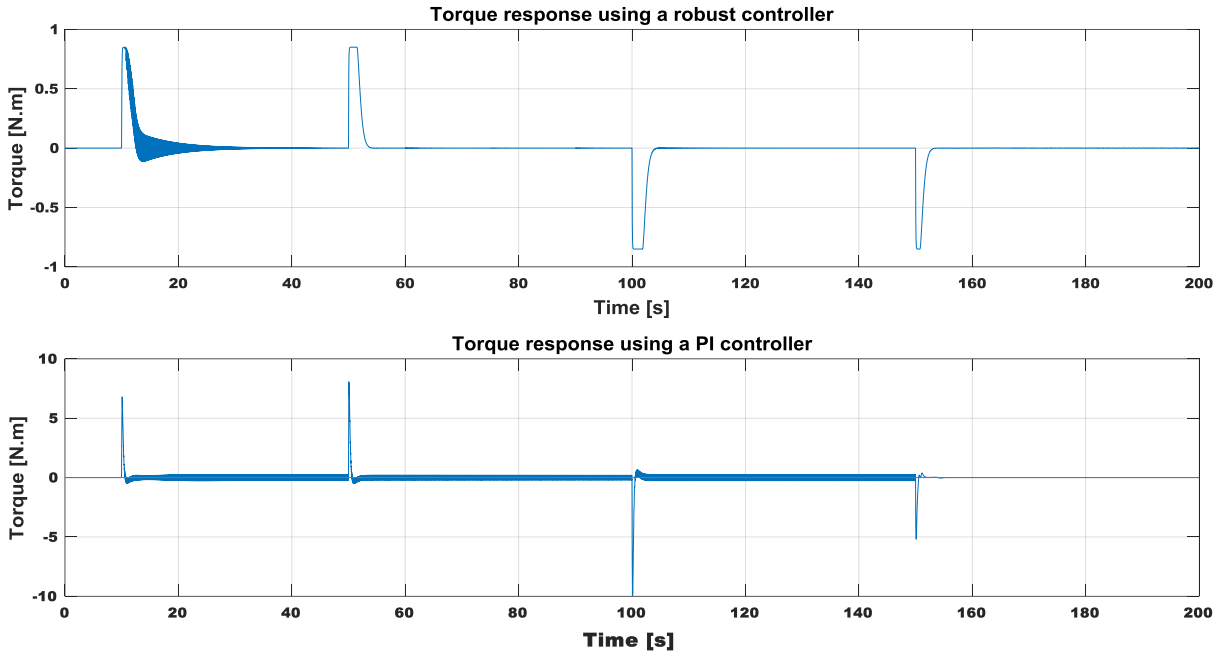

c) Torque Responses en [N.m]

Figure 13. A comparative study of conventional PI and H_∞ anti-windup controllers for direct vector control applied to an asynchronous motor

The responses in Figure 13 represent the simulation of the vector control applied to the asynchronous motor. This study is performed by two types of controllers, such as the Proportional Integral controller and a robust H_∞ Antiwindup controller. Indeed, the use of a robust H_∞ Antiwindup controller allows for the improvement of the performances of the vector control such as the response time, the overshoot, and the ripples of the quantities. These improvements allow the optimization of the power consumption by the drive train. The simulation of the classical vector control based on PI controllers applied on an asynchronous motor in the drive train is shown in Figure 13; the variation of the speed at certain times causes peaks in the electromagnetic torque.

In the simulation shown in Figure 13, the speed of the vehicle on the motorway is varied from zero to 110km/h, these variations allow the performance of the conventional vector control applied to the vehicle to be tested. The variations in speed and the application of the resistive torque cause peaks in the responses of various machine variables. Indeed, this vector control technique does not allow the optimization of the vehicle's energy consumption because of the proportional-integral controllers used, whose syntheses do not take into account the variation of the motor parameters and external disturbances. In order to improve the performance and to ensure a good optimization of the energy consumed by the vehicle, as well as to ensure peak attenuation, the H_∞/anti windup control strategy applied to rotor flux vector control is adopted in the following section.

4- Test Bench for the Traction Chain

An electric traction chain is composed mainly of a power part that provides the electromechanical conversion of energy and a control part that controls the power switches.

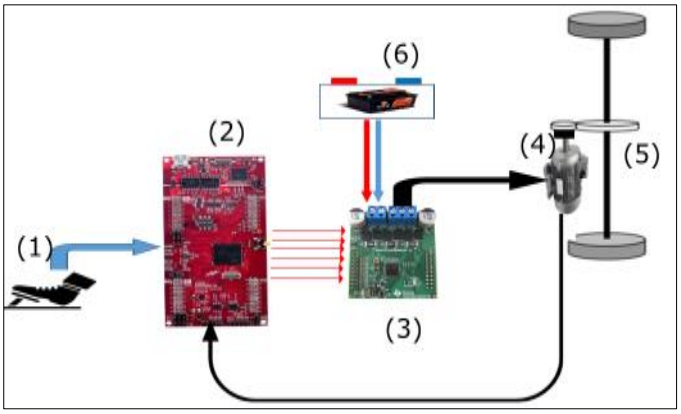

Figure 14. Traction Chain

In Figure 14:

- The traction power for the wheels is provided by *the three-phase electric machine (4)*.
- The torque of the wheels is provided by a *differential (5)* with a gear ratio to adapt the speed of the machine shaft to that of the wheels
- The torque and speed of the machine are controlled by *the inverter (3)* which converts the DC voltage from *the* ***battery (6)*** into a three-phase AC voltage suitable for the electric machine
- The energy flow is managed by *the control unit (2)*, which converts *the driver's commands (1)* to controls sent to the power unit.

The experimental bench contains a control part based on the TMS320F28379D DSP from Texas Instrument, and a power part realized by a low voltage converter BOOSTXL-DRV8305EVM:

- The TMS320F28379D DSP is a dual processor CPU based on TI's 32-bit C28x architecture. Each core can access its own local RAM, flash memory and shared RAM. The Interprocessor Communication Module (IPC) provides data sharing between the two CPUs. Each CPU operates at 200 MHz. [18, 19].
- The BOOSTXL-DRV8305EVM is a module that provides a DC bus and phase voltage detection as well as an individual current shunt for sensorless BLDC algorithms. The module supplies the MCU with 3.3V with a 0.6A LMR16006 step-down regulator.
- The control and power stages are fully protected by short-circuit, heat, discharge and thermal undervoltage protections, (Figure 15) [18].

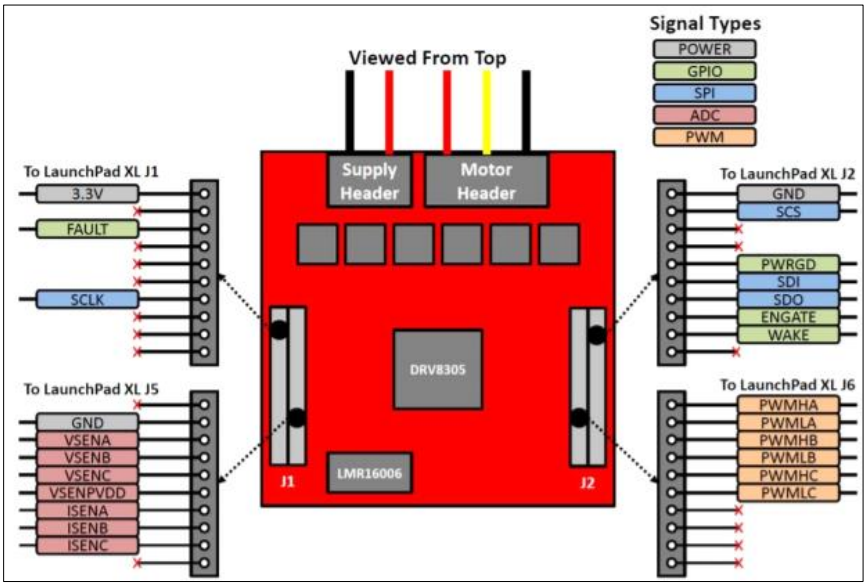

Figure 11. BOOSTXL-DRV8305EVM pinout

4-1- Experimental Design and Discussion

To validate the use of the proposed procedure for the simultaneous estimation of asynchronous motors, the simulation results must be compared with experimental tests [20]. In this section, we worked on the acquisition of voltages and currents. From these practical measurements, we can estimate the variables of the induction motor such as the flux, the pulsation $\omega_s$and the motor′s angular speed Ω_r (Figure 16). These measurements are based on the use of voltage and current sensors.

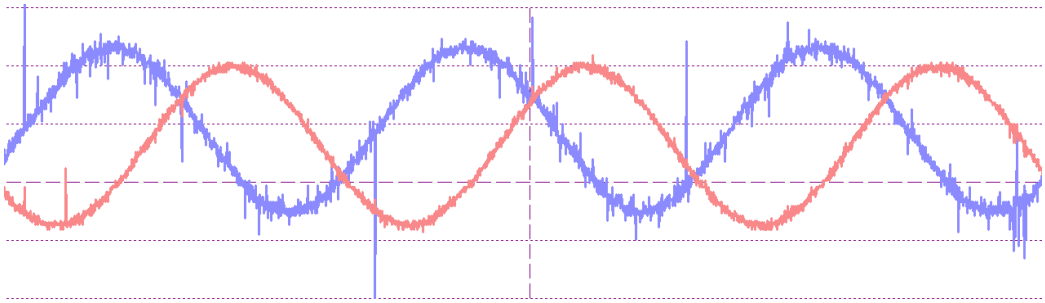

Figure 12. Sensor Current Signal

The practical test bench used to implement the asynchronous control algorithms is shown in Figure 17. The nominal motor parameters are (1.1kW, 50 Hz, p=2, Rs=6.75Ω, Rr=6.21Ω, Ls=Lr=0.5192 H, Msr= 0.4957 H, f=0.002 SI, J=0.01240 kg.m²). Figure 17 shows the experimental structure in real-time.

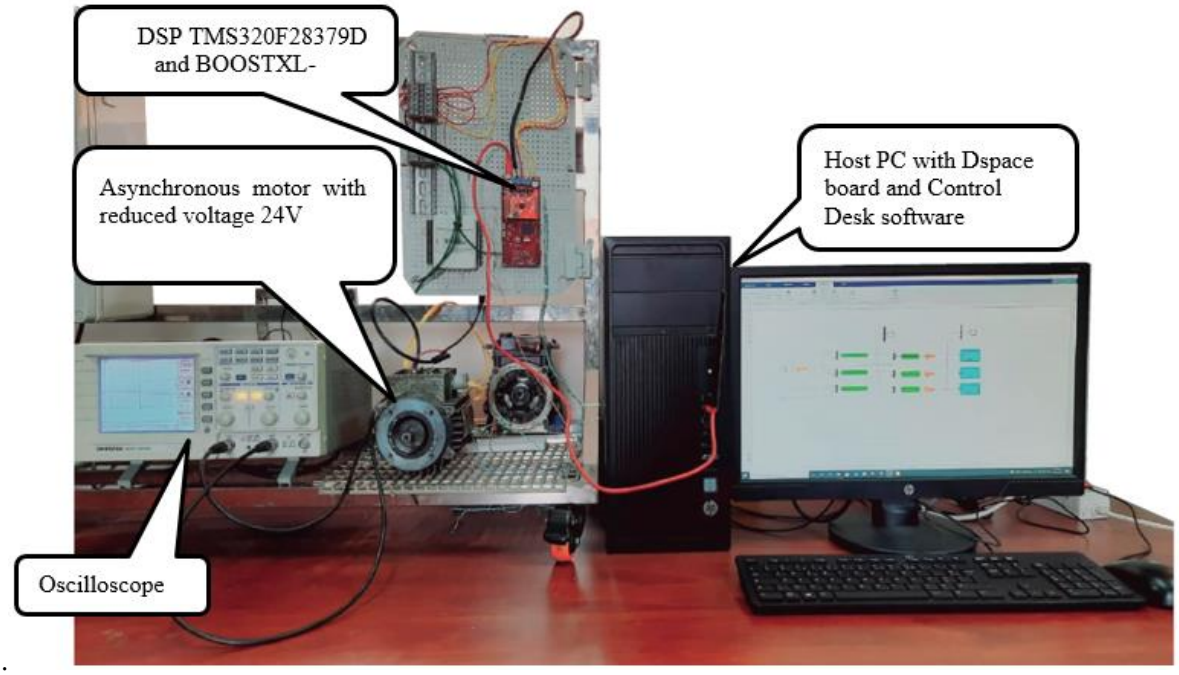

Figure 13. Photo of the traction chain test bench

4-1-1- Simulink Program

The Simulink program in Figure 18 represents real-time tests of the vector PWM control applied to an asynchronous motor with reduced voltage (24v) adapted to the embedded board.

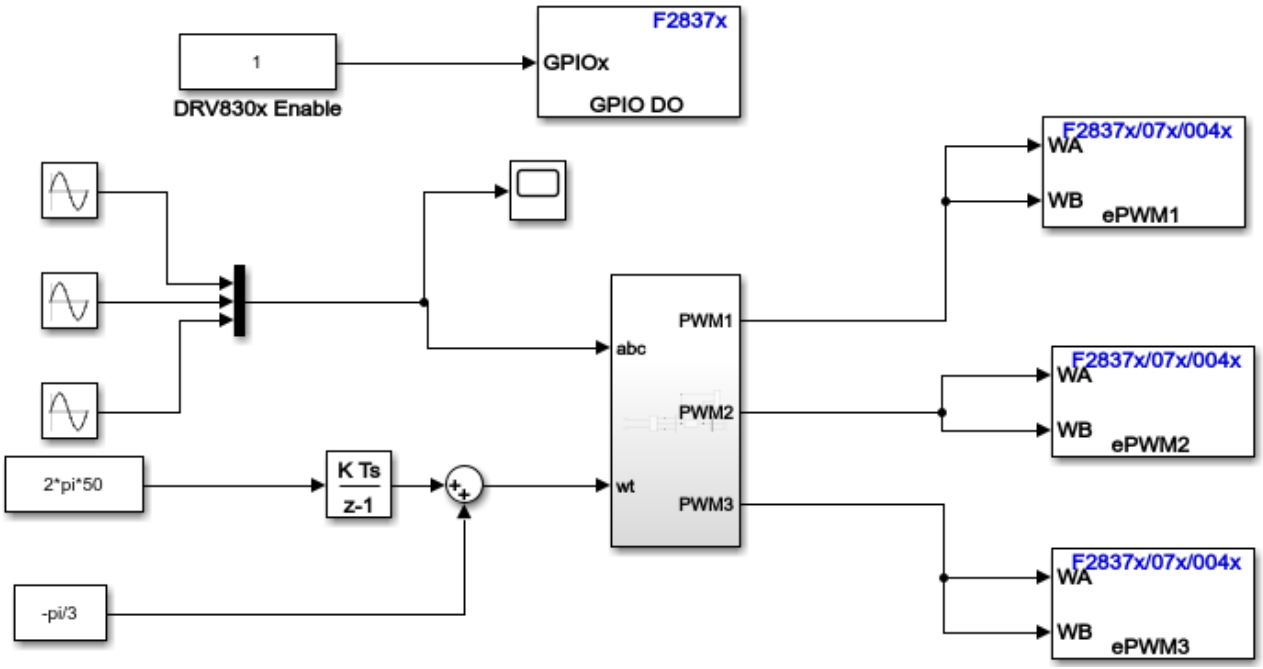

Figure 14. Example of a Matlab/Simulink program to control the asynchronous machine

4-1-1- PWM Experimental Response

The program in Figure 18 allows to visualize in real time the PWMs used to control the six switches of the BOOSTXL-DRV8305EVM voltage inverter. Figure 19 shows the PWMs of phase *A* [21].

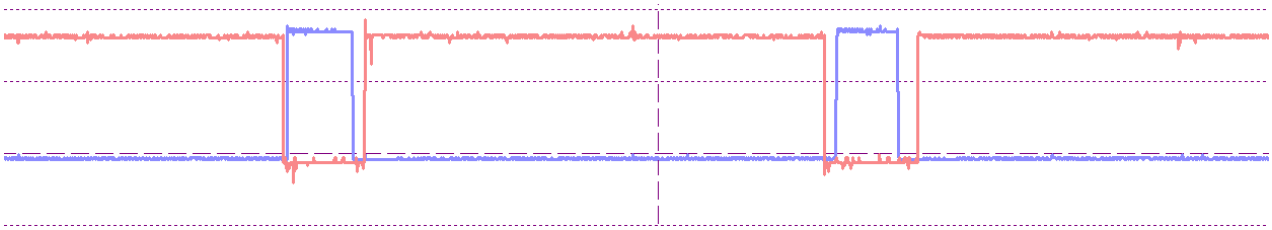

Figure 15. PWM of phase A

5- Conclusion

This study presents a comparative evaluation of two conventional PI controllers and a vector H_∞ Antiwindup control applied on the asynchronous motor of the drive train. A conventional method based on the use of conventional PI controllers of three parameters such as flux, speed, and torque was developed and simulated for different operating conditions. To evaluate the performance of this control, an H_∞ Antiwindup controller replaces the speed PI controller. The test results indicate that improvements were achieved for speed, flow, and torque. In addition, the Anti-windup vector control provides better dynamic control under different operating conditions, such as steady-state, load application, and low-speed operation. This modified technique preserves the good properties of classical vector control as a simple scheme designed within a stationary framework.

In general, the insertion of the Antiwindup technique into the vector control scheme solves the most common drawbacks of vector control. Several comparable analyses and validations verify that the proposed method can achieve good velocity tracking performance and strong robustness to external load disturbances and parameter variation. Further research could focus on the design of the dynamic H_∞ controller including dq axis current performance with more accurate decoupling methods.

Using MATLAB Simulink embedded coding tools saves time and money, is more efficient, has faster execution time, and is ideal for industrial control research and design. The programming of the TMS320F28379D microcontroller with its BOOSTXL-DRV8305EVM using the embedded approach in MATLAB Simulink is developed in this paper, using tests under different operation conditions.

6- Declarations

6-1- Author Contributions

A.B., M.C., D.B., and K.R. contributed to the design and implementation of the research, to the analysis of the results and to the writing of the manuscript. All authors have read and agreed to the published version of the manuscript.

6-2- Data Availability Statement

The data presented in this study are available in the article.

6-3- Funding

The authors received no financial support for the research, authorship, and/or publication of this article.

6-4- Conflicts of Interest

The authors declare that there is no conflict of interest regarding the publication of this manuscript. In addition, the ethical issues, including plagiarism, informed consent, misconduct, data fabrication and/or falsification, double publication and/or submission, and redundancies have been completely observed by the authors.

7- References

[1] El Amrani, S., Chennani, M., & Belkhayat, D. (2019). Comparative Study of Electric Vehicle Energy Consumption between Trunk Roads and Highways. Proceedings of 2019 7th International Renewable and Sustainable Energy Conference, IRSEC 2019, 1–7. doi:10.1109/IRSEC48032.2019.9078169.

[2] Ye, F., Wu, G., Boriboonsomsin, K., & Barth, M. J. (2016). A hybrid approach to estimating electric vehicle energy consumption for ecodriving applications. IEEE Conference on Intelligent Transportation Systems, Proceedings, ITSC, 719–724. doi:10.1109/ITSC.2016.7795633.

[3] Wu, X., Freese, D., Cabrera, A., & Kitch, W. A. (2015). Electric vehicles' energy consumption measurement and estimation. Transportation Research Part D: Transport and Environment, 34, 52–67. doi:10.1016/j.trd.2014.10.007.

[4] Yao, E., Wang, M., Song, Y., & Zhang, Y. (2014). Estimating energy consumption on the basis of microscopic driving parameters for electric vehicles. Transportation Research Record, 2454, 84–91. doi:10.3141/2454-11.

[5] Lü, X., Qu, Y., Wang, Y., Qin, C., & Liu, G. (2018). A comprehensive review on hybrid power system for PEMFC-HEV: Issues and strategies. Energy Conversion and Management, 171, 1273–1291. doi:10.1016/j.enconman.2018.06.065.

[6] Wang, Y., Sun, Z., Li, X., Yang, X., & Chen, Z. (2019). A comparative study of power allocation strategies used in fuel cell and ultracapacitor hybrid systems. Energy, 189, 116142. doi:10.1016/j.energy.2019.116142.

[7] Zhou, D., Al-Durra, A., Gao, F., Ravey, A., Matraji, I., & Godoy Simões, M. (2017). Online energy management strategy of fuel cell hybrid electric vehicles based on data fusion approach. Journal of Power Sources, 366, 278–291. doi:10.1016/j.jpowsour.2017.08.107.

[8] Kumar, M., & Moulik, B. (2021). Dynamic modeling and analysis of control techniques of an induction motor drive for application in an electric vehicle. Proceedings - IEEE 2021 International Conference on Computing, Communication, and Intelligent Systems, ICCCIS 2021, 1037–1042. doi:10.1109/ICCCIS51004.2021.9397093.

[9] Wei, H., Fan, L., Ai, Q., Zhao, W., Huang, T., & Zhang, Y. (2022). Optimal energy allocation strategy for electric vehicles based on the real-time model predictive control technology. Sustainable Energy Technologies and Assessments, 50, 101797. doi:10.1016/j.seta.2021.101797.

[10] Boudallaa, A., Chennani, M., Rhoufir, K., & Belkhayat, D. (2020). Practical Estimation of Rolling Energy of an Electric Vehicle using onboard GPS (No. 2462). EasyChair.

[11] Abdelati, R., & Faouzi Mimouni, M. (2011). Analytical Solution of Optimized Energy Consumption of Induction Motor Operating in Transient Regime. European Journal of Control, 17(4), 397–411. doi:10.3166/ejc.17.397-411.

[12] Bernard, J. (2007). Véhicules hybrides à pile à combustible: dimensionnement et stratégies de commande. Ph.D. Dissertation, University of Valenciennes and Hainaut-Cambresis, Valenciennes, France. (In French).

[13] Et-Taaj, L., Boulghasoul, Z., Elbacha, A., & El Kharki, A. (2021). Robust sensorless Induction Motor control based on Extended Kalman Filter observer. 2021 International Congress of Advanced Technology and Engineering, ICOTEN 2021, 1–9. doi:10.1109/ICOTEN52080.2021.9493502.

[14] Abdelati, R., & Mimouni, M. F. (2019). Optimal control strategy of an induction motor for loss minimization using Pontryaguin principle. European Journal of Control, 49, 94–106. doi:10.1016/j.ejcon.2019.02.004.

[15] Boulghasoul, Z., Kandoussi, Z., Elbacha, A., & Tajer, A. (2020). Fuzzy Improvement on Luenberger Observer Based Induction Motor Parameters Estimation for High Performances Sensorless Drive. Journal of Electrical Engineering and Technology, 15(5), 2179–2197. doi:10.1007/s42835-020-00495-6.

[16] Attaianese, C., Perfetto, A., & Tomasso, G. (1999). Robust position control of DC drives by driveof H/sub/spl infin/SPLntrollers. IEE Proceedings-Electric Power Applications, 146, 391–396. doi:10.1049/ip-epa:19990342.

[17] Rigatos, G., Siano, P., Wira, P., & Profumo, F. (2015). Nonlinear H-infinity Feedback Control for Asynchronous Motors of Electric Trains. Intelligent Industrial Systems, 1(2), 85–98. doi:10.1007/s40903-015-0020-y.

[18] Boulmane, A., Zidani, Y., & Belkhayat, D. (2018). Implementation of Modulation Techniques on TMS320F28379D Launchpad Using the BOOSTXL-DRV8305EVM. 2018 International Symposium on Advanced Electrical and Communication Technologies (ISAECT). doi:10.1109/isaect.2018.8618756.

[19] Da Fonseca, B. S., & Andres Santisteban, J. (2019). An Electronic Drive for a Switched Reluctance Motor Using a DSC. 2019 IEEE 15th Brazilian Power Electronics Conference and 5th IEEE Southern Power Electronics Conference, COBEP/SPEC 2019, 1–6. doi:10.1109/COBEP/SPEC44138.2019.9065302.

[20] Alouane, A., Rhouma, A. B., & Khedher, A. (2018). FPGA Implementation of a New DTC Strategy Dedicated to Delta Inverter-Fed BLDC Motor Drives. Electric Power Components and Systems, 46(6), 688–700. doi:10.1080/15325008.2018.1461148.

[21] Elrajoubi, A., Ang, S. S., & Abushaiba, A. (2017). TMS320F28335 DSP programming using MATLAB Simulink embedded coder: Techniques and advancements. 2017 IEEE 18th Workshop on Control and Modeling for Power Electronics, COMPEL 2017 (pp. 1–7). doi:10.1109/COMPEL.2017.8013418.